ACERP: Vol. 6, No. 1, (Winter 2020) 43-48

Advanced Ceramics Progress

Research Article

Journal Homepage: www.acerp.ir

Crystal Structure and Lattice Parameter Investigation of La^{3+} Substituted CeO_2 in $La_xCe_{1-x}O_{2-X/2}$ Synthesized by Solid-State Method

A. M. Fathi Dehkharghani [a], M. R. Rahimipour [a], M. Zakeri [a *]

[a] *Ceramics Department, Materials and Energy Research Center, Meshkin Dasht, Alborz, Iran*

PAPER INFO

Paper history:

Received 16 December 2019
Accepted in revised form 3 February 2020

Keywords:

$La_2Ce_2O_7$
Solid State
Synthesize
Crystal Structure
Lattice Parameters

ABSTRACT

Lanthanum (La) doped Ceria (CeO_2) has attracted considerable interest as a candidate material for thermal barrier coating (TBC) because of its low thermal conductivity and potential capability to be operated above 1250°C. In this study, $La_2Ce_2O_7$ powder was synthesized through the ball mill method. The crystal structure of La^{3+} substituted CeO_2 solid solution was investigated by X-ray diffraction in $La_xCe_{1-x}O_{2-x/2}$ ($0<x<0.5$). The fluorite structure of CeO_2 did not change although La^{3+} was the largest trivalent rare-earth ion. The lattice parameter changed from 5.41 to 5.59Å by increasing La content. Changes in the lattice parameters of $La_xCe_{1-x}O_{2-x/2}$ that were compared with the theoretical values measured by XRD were obtained based on the oxygen vacancy model. The theoretical lattice parameters were larger than the lattice parameters calculated from the X-ray diffraction pattern. Moreover, the Williamson–Hall equation was used to measure the crystallite size and strain in the $La_xCe_{1-x}O_{2-x/2}$ lattice as a function of the lanthanum content. The results showed that the presence of lanthanum in the structure reduced the crystallite size.

1. INTRODUCTION

Rare-earth metals (RE)-doped ceria with fluorite structures have recently been at the center of attention, particularly due to their unique combination of electrical, catalytic, and mechanical properties [1,2]. Increased chemical stability and ion conductivity of RE-doped ceria-based materials are mainly attributed to the replacement of Ce^{4+} ions with La^{3+}, Sm^{3+}, and Gd^{3+} ions. Such a unique combination of properties cause RE-doped ceria ceramics proposed as promising candidates for much application including solid oxide fuel cells (SOFC), oxygen sensors, and catalysts [3-7]. Additionally, due to properties such as high melting point, low thermal conductivity, high coefficient of thermal expansion (CTE), favorable chemical and thermal stability, strong adhesion to metallic substrates, and low sinterability, RE-doped ceria-based ceramics are widely used as thermal barrier coatings (TBC) [8-10].

Several methods have been proposed for $La_2Ce_2O_7$ synthesis, including sol-gel, solid-State reactions, hydrothermal treatments (for 24 hours in 180°C), pressure-less sintering sol-gel (PSSG) in 1600°C for 10h, atmospheric plasma spray, electron beam physical vapor deposition (EBPVD), and high-temperature solid-state method [11,12].

High-purity (>99.99%) lanthanum oxide and cerium oxide powders were used as raw materials for the synthesis of $La_2Ce_2O_7$ bulk ceramics by Wen Ma et. al [13]. The material was sintered at 1600°C for 6 hours and the corresponded CTE was measured through the thermal cycle of 180°C.h^{-1}.

The solid-state reaction method was used by Jong Sung Bae et al. to synthesis the $La_xCe_{1-x}O_{2-x/2}$ ceramics from La_2O_3 and CeO_2 precursors, at 1400°C for 7 hours. They achieved an XRD pattern at room temperature implying a high symmetry that confirmes the formation of single-phase by calcining the mixture of constituent oxide from x=0-0.4 [7].

The structural study of La^{3+} substituted CeO_2, $La_xCe_{1-x}O_{2-x/2}$ solid solution has been investigated. La^{3+} has the largest size among the trivalent rare-earth ions such that the size difference between Ce^{4+} and La^{3+} is large [7,11,14]. In the case of +3/+4 oxides, the pyrochlore structure is favored, where a cation radii ratio r_A/r_B is greater than 1.42. It is also observed that the disordered fluorite structure is favorable at lower r_A/r_B value. Since

* Corresponding Author Email: m_zakeri@merc.ac.ir (M. Zakeri)

the ionic radii of eight-coordinated La^{3+} is 1.30Å, and eight -coordinated Ce^{4+} is 0.97Å, so r_A/r_B=1.36. Therefore, it is expected that the fluorite structure should be observed for the mixed oxide made out of Ce^{4+} and La^{3+}. Moreover, recent studies suggest that the rare-earth doped ceria ($La_2Ce_2O_7$) has disordered defect fluorite structure [1,11,15,16]. This paper initially concerned the process of synthesizing $La_2Ce_2O_7$ powder by the ball mill method and examined the effect of milling time and heat treatment on the synthesize process. Then, the effect of changing the amount of lanthanum is investigated in the oxide mixture of $La_xCe_{1-x}O_{2-x/2}$ for $0<x<0.5$ on the crystal structure, crystal size, and lattice parameter. The X-ray diffraction analysis (XRD) is used to examine the microstructure of the present phases and Energy Dispersive X-ray spectroscopy (EDS) is used to verify the stoichiometric composition.

2. MATERIALS and METHOD

CeO_2 and La_2O_3 (99.5%) powders, products of Strategic Elements Co. were used as raw materials for the solid-state synthesis of LC. The powder mix—48% lanthanum oxide and 52% cerium oxide—was milled for 20 hours at 300rpm in a zirconia cup with 10:1 zirconia ball to powder ratio, and then heat-treated at 1300°C for 3 hours. The $La_xCe_{1-x}O_{2-x/2}$ (x = 0.1, 0.2, 0.3, 0.4, and 0.5) solid solution with different ratios of La_2O_3 and CeO_2 were synthesized to investigate the crystal structure and to study the effect of changing the Lanthanum content on the lattice parameter and crystallite size.

The crystal structures and lattice parameters of the synthesized solid solutions were studied using a Philips pw3710 diffractometer, and the chemical composition of the LC was investigated by EDS analysis. The crystallite size and strain in the $La_xCe_{1-x}O_{2-x/2}$ lattice were calculated using the Williamson–Hall equation because the broadening of the peak can be partially attributed to the finer crystallite and partially to the increased lattice strain. The crystallite size was also obtained from the Scherrer equation:

$$\beta = \lambda.K/D \cos\theta \quad (1)$$

Where, λ represents the wavelength of the X-ray, θ is the diffraction angle, K is a constant (0.9), β shows the Full Width at Half Maximum (FWHM) for the highest peak.

$$\beta_b^2 = B^2 - b^2 \quad (2)$$

The FWHM of the specimen is denoted by B, whereas b represents the FWHM for a standard silicon reference specimen [17].

According to the Scherrer equation, the broadening of the peak is a result of the crystallite size. However, the strain developing in the lattice is also a culprit of the broadening of the peak. The lattice-strain-induced change in the width of the peak can be calculated from Eq. 3:

$$\beta_S = 2A\varepsilon \tan\theta \quad (3)$$

According to these equations, the total peak broadening is:

$$B = \beta_D + \beta_S \quad (4)$$
$$\beta = \lambda.K/D \cos\theta + 2A\varepsilon \tan\theta \quad (5)$$

By multiplying both sides in cos θ, it would be:

$$\beta \cos\theta = \lambda.K/D + 2A\varepsilon \sin\theta \quad (6)$$

Equation 6 is the Williamson–Hall (W–H) equation where ε represents the lattice strain and A is a constant (often 1). In the general form of the equation, the slope shows the lattice strain, whereas the vertical intercept is used to estimate the crystallite size [18].

3. RESULTS and DISCUSSION

3.1. X-Ray diffraction

Figure 1 shows the X-ray diffraction (XRD) patterns of the synthesized LC powder. The resulting diffraction pattern resembles the cubic fluorite CeO_2, but shifted to smaller angles with no peak corresponding to La_2O_3, indicating the formation of the $La_2Ce_2O_7$ solid solution. The resulting pattern is a basic reflection with no additional peaks, showing only one phase after the synthesis. Therefore, the CeO_2 can fully incorporate the larger La^{3+} ions, while preserving its fluorite structure.

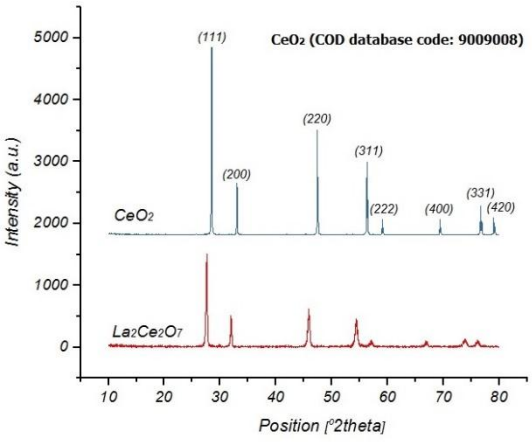

Figure 1. The X-ray diffraction patterns of CeO_2 and synthesized $La_2Ce_2O_7$ powder

The EDS analysis of the LC powder (Fig. 2) also indicates 64.35 at.% oxygen, 17.46 at.% lanthanum, and 17.79 at.% cerium in the chemical composition, which is similar to the stoichiometric ratio of the $La_2Ce_2O_7$.

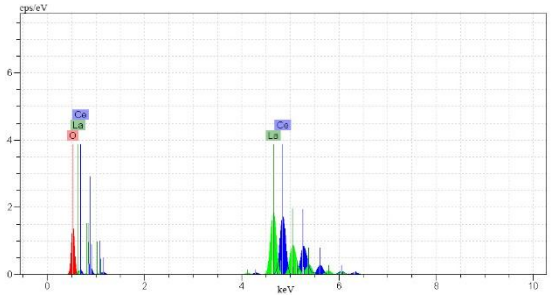

Figure 2. The EDS analysis of the synthesized LC powder

Fig. 3 shows the XRD patterns for $La_xCe_{1-x}O_{2-x/2}$ (x = 0.1, 0.2, 0.3, 0.4, and 0.5) and pure cerium oxide (x = 0).

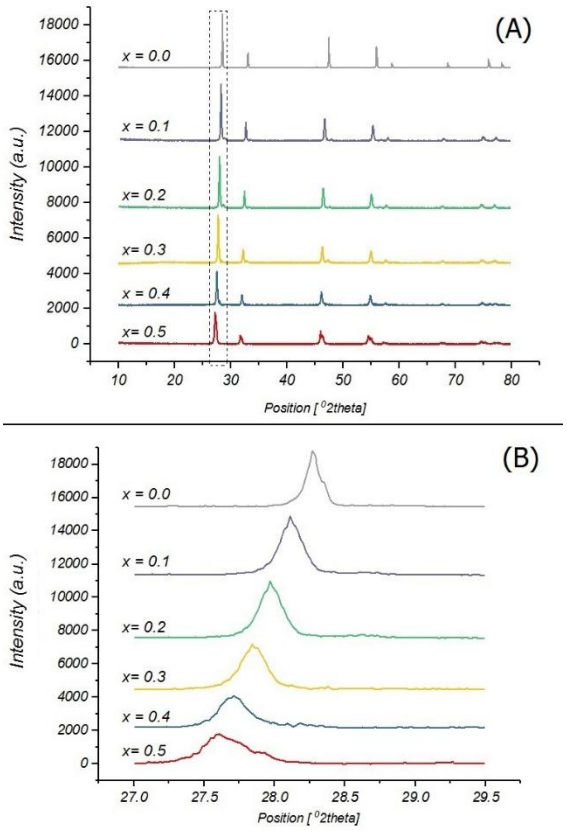

Figure 3. The X-ray diffraction patterns for $La_xCe_{1-x}O_{2-x/2}$ as a function of x

As evident from the Fig. 3 (A), all oxide mixes exhibit shifted fluorite ceria patterns (Fig. 3(B)).

No secondary phase or additional peaks is found in the powder mixes, indicating the formation of a homogeneous oxide phase. This implies that the CeO_2 structure can completely incorporate the larger La^{3+} ions in its lattice and still maintains its fluorite structure despite the La^{3+} substitution. The diffraction patterns further shift to smaller angles as a result of the change in the lattice parameter by increasing the La content [11,14,19,20].

3.2. Crystallite size

One thing to note in Fig. 3 is the broadening of the peaks by adding La, which is suggestive of a reduction in crystallite size at higher La contents. Therefore, adding La impedes the growth of ceria crystals [11,14].

Considering the growth mechanism of ceria is required to rationalize the observed decline of the crystallite size with La content.

The synthesis process includes two major steps; the formation of stable nucleus and crystal growth through the Oswald Ripening (OR) or oriented attachment (OA) mechanism [21,22].

It is expected that the replacement of host cations with dopant ions in ceria influences the thermodynamic and kinetic of the growth process. The growth mechanism of the ceria particles should also be illustrated to indicate the effect of increased La content on decreasing the crystallite size. Considering OA as the dominant growth mechanism and removing the high energy surfaces (the driving force of OA mechanism) can cause a significant decrease in the surface free energy. Consequently, Van der Waals (VW) forces can cause sufficiently close crystals to absorb each other [23,24]. Ivanov et al. reported that the decreased crystallite size of ceria with an increasing fraction of dopant can be well described through the delayed ceria crystallite growth, which is promoted by the segregation of dopant ions at the surface. Such surface segregation causes decreased surface energy of the particles and consequently, restricts the OA mechanism (derived by high-energy surfaces) [24].

However, the mentioned surface segregation mechanism cannot be used in this case due to the homogenous distribution of La in CeO_2 particles. Therefore, a simplified model has been used to illustrate the effects of the replacement of La^{3+} ions with Ce^{4+} ions through the OA growth mechanism. The model includes two N×N arrays of nodes as the rectangular crystalline planes. Each node consists of x mole A (dopant) atoms and 1-x mole B (host) atoms. The average distance between the nodes is defined as the lattice parameter, which may be different for different planes, as the number of A and B atoms are different in each crystalline plane [24].

Strong chemical bonding can be formed between the plans if the number of similar atoms in atomic rows of two adjacent planes does not show a significant

difference. In other words, the atomic rows of each plane can fit together when the difference between the numbers of atoms in each row did not exceed the m factor. Such a parameter is defined as the difference between the lattice parameters of pure A and B can be calculated as follows [24]:

$$m \approx d/\Delta d \quad (7)$$

Whereas, d shows the lattice parameter in Eq. 7, the probability of row fitting (P_1) can be calculated via the following formula [24]:

$$P_1 \approx m[\pi x(1-x)N]^{-1/2} \quad (8)$$

Eq. 8 has been derived from the calculations of the probability theory, based on the presence probability (PP) of A and B atoms in rows accompanied with considerations such as $d>>\Delta d$ and $N>>1$. Whereas the presence probability (PP) in a row is considered as x for A atoms and the PP for B should be considered as 1-x [24].

P_2 is defined as the fitting probability of two perpendicular rows in one plane with the other planes. This parameter can be considered as the square of P_1 and calculated as follows [24]:

$$P_2 \approx m[\pi x(1-x)N]^{-1} \quad (9)$$

If the condition $P_2 \approx 1$ is considered as the criterion for the stopped particle growth, the indexed parameter of particle size (D=Nd) can be calculated through the following equation [24]:

$$D \approx [\pi x(1-x)]^{-1}(d/\Delta d)^2 d \quad (10)$$

Eq. 10 clearly illustrates that the particle size is decreased by the increased fraction of dopant (x). As the OA process intrinsically includes the formation of crystalline defects such as twinning, porosities and surface disorders, other processes such as recrystallization and OR should be occurred to decrease the lattice defects.

The high cohesion energy of ceria causes a slow recrystallization process through surface diffusion mechanism. Therefore, it seems that the atomic movements majorly occurr through the OR process, which confirms the important role of the OR process in addition to OA [24,25].

It must be noted that both the particle size and the lattice strain broaden the XRD peaks [11,14,19].

Lattice strain also affects the peak width considering that the W–H equation was used to calculate the crystallite size and lattice strain besides changing the crystallite size. The W–H equation is first-order, and its slope and intercept yield the lattice strain and the crystallite size. Table 1 shows the crystallite sizes and lattice strains obtained from the W–H equation for $La_xCe_{1-x}O_{2-x/2}$ compounds as a function of x. The results show that the incorporation of La into the structure reduces the crystallite size.

TABLE 1. Crystallite sizes and lattice strains of the synthesized compounds

x in $La_xCe_{1-x}O_{2-x/2}$	Crystallite Sizes (nm)	Lattice Strains (%)	R^2
x=0	115.6	0.0016	0.9531
x=0.1	99.1	0.0023	0.9137
x=0.2	86.7	0.0026	0.8068
x=0.3	77.0	0.0030	0.9119
x=0.4	69.4	0.0034	0.8972
x=0.5	63.0	0.0038	0.9073

Figure 4 shows the variations of crystallite size and lattice strain as a function of La content. As evident, the lattice strain increases by raising the La content. The La^{3+} forms oxygen vacancies in the CeO_2 lattice, converting the Ce^{4+} cations to Ce^{3+}. The conversion changes the local symmetry in the lattice, which in turn, changes the Ce–O bond length [18,26]. Further, the La^{3+} cation with a larger ionic radius also disturbs the local symmetry of the lattice. All the above contribute to the increase in the lattice strain when La is introduced to the structure.

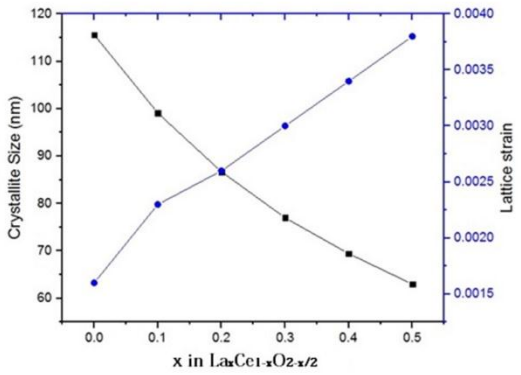

Figure 4. Lattice strain and crystallite size variations in $La_xCe_{1-x}O_{2-x/2}$ compounds as a function of x

3.3. Lattice parameter

In this study, the XRD patterns, experimental lattice constant results, and the oxygen vacancy model were used to calculate the theoretical lattice parameter for the $La_xCe_{1-x}O_{2-x/2}$ powder, and the results were compared. Equation 11 was used to calculate the lattice parameter of the cubic structure based on XRD patterns.

$$1/d^2 = (h^2+k^2+l^2)/a^2 \quad (11)$$

d: Spacing of crystal planes
h k l: Miller indices
a: Lattice parameter

Theoretical lattice parameter results were calculated based on the oxygen vacancy model using Eq. 12 [7].

$$a = 4/\sqrt{3}\ [r_M - r_{Ce} - 0.25_{ro} + 0.25_{rvo}]x + 4/\sqrt{3}\ [r_{Ce} + r_o] \quad (12)$$

$M = La^{3+}$
$Ce = Ce^{4+}$
$O = O^{2-}$
V_o = oxygen vacancy

Fig. 5 plots the changes in the lattice parameter calculated from diffraction patterns and the theoretical lattice parameter calculated based on the oxygen vacancy model as a function of the La dopant content.

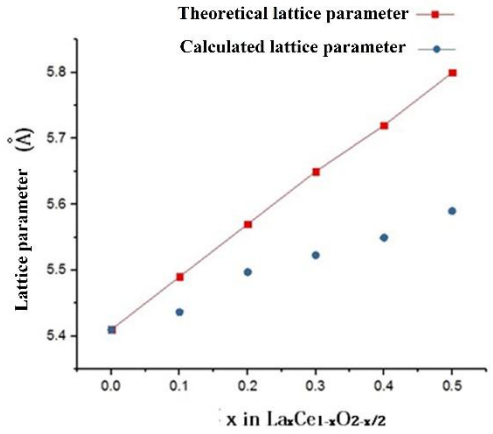

Figure 5. Changes in the lattice parameter as a function of the La dopant concentration

As evident, the lattice parameter increases by further adding of La. The substitution of Ce^{4+} with La^{3+} in the lattice enlarges the octahedral face in the lattice of the cubic fluorite CeO_2, which also increases the lattice parameter in $La_2Ce_2O_7$. The shift of CeO_2 peaks to smaller angles in Fig. 3 also verifies this phenomenon [11,12].

As evident from Fig. 5, the theoretical lattice parameters were larger than the lattice parameters calculated based on XRD patterns. Further, the discrepancy between the experimental and theoretical results increases by adding La. The discrepancy shows that the volume of the fluorite unit cell can shrink as a result of the joining the vacancies. Further, given that the number of vacancies increased by the addition of La and the contraction is also exacerbated by increasing the difference between the theoretical and experimental lattice parameters [7].

In conclusion, two factors control fluorite lattice parameters. The first is the size difference between La^{3+} and Ce^{4+} ions. Note that La^{3+} has a larger ionic radius than the Ce^{4+}, thus increasing the lattice parameter (a). The second less significant factor is the defects in the crystal lattice that contract the unit cell.

4. CONCLUSIONS

1. In $La_2Ce_2O_7$ compounds, where x is between 0.1 and 0.5, the CeO_2 structure can embed the larger La^{3+} ions in its lattice, while preserving its fluorite structure. Changing the La content of the compound resulted in a shift in diffraction patterns due to the different lattice parameters and the broadening of the peaks as a result of the reduced particle size.
2. The La^{3+} formed oxygen vacancies in the CeO_2 lattice, converting the Ce^{4+} cations to Ce^{3+}. The conversion changed the local symmetry in the lattice, which in turn, changed the Ce–O bond length. Further, the La^{3+} cation with a larger ionic radius also disturbed the local symmetry of the lattice. All the above contributed to the increase in the lattice strain when La is introduced to the structure.
3. The theoretical lattice parameters were larger than the lattice parameters calculated based on XRD patterns. Further, the discrepancy between the experimental and theoretical results increased by adding La. Given that increasing the La content increases the number of vacancies, the contraction induced by the joining of vacancies and the difference between the theoretical and experimental lattice parameter results also increased.

5. ACKNOWLEDGEMENTS

Authors would like to thank the Materials and Energy Research Center for financial support of this research.

REFERENCES

1. Tinwala, H., Shah, D. V., Menghani, J., Pati, R., "Synthesis of $La_2Ce_2O_7$ Nanoparticles by Co-Precipitation Method and Its Characterization", ***Journal of Nanoscience and Nanotechnology***, Vol. 14, No. 8, (2014), 6072–6076.
2. Pati, R. K., Iee, I. C., Hou, S., Akhuemonkhan, O., Gaskell, K. J., Wang, Q., Frenkel, A. I., Chu, D., Salamanca-Riba, L. G., Ehrman, S. H., "Flame Synthesis of Nanosized Cu−Ce−O, Ni−Ce−O, and Fe−Ce−O Catalysts for the Water-Gas Shift (WGS) Reaction", ***ACS Applied Materials & Interfaces***, Vol. 1, No. 11, (2009), 2624–2635.

3. Wang, C., Huang, W., Wang, Y., Cheng, Y., Zou, B., Fan, X., Yang, J., Cao, X., "Synthesis of Monodispersed $La_2Ce_2O_7$ Nanocrystals via Hydrothermal Method: A Study of Crystal Growth and Sintering Behavior", ***International Journal of Refractory Metals and Hard Materials***, Vol. 31, (2012), 242–46.
4. Wang, Y., Guo, H., Gong, S., "Thermal Shock Resistance and Mechanical Properties of $La_2Ce_2O_7$ Thermal Barrier Coatings with Segmented Structure", ***Ceramics International***, Vol. 35, No. 7, (2009), 2639–2644.
5. Gill, J. K., Pandey, O. P., Singh, K., "Ionic Conductivity, Structural and Thermal Properties of Ca^{2+} Doped $Y_2Ti_2O_7$ Pyrochlores for SOFC", ***International Journal of Hydrogen Energy***, Vol. 37, No. 4, (2012), 3857–3864.
6. O'neill, W. M., Morris, M. A., "The Defect Chemistry of Lanthana–Ceria Mixed Oxides by MASNMR", ***Chemical Physics Letters***, Vol. 305, No. 5–6, (1999), 389–394.
7. Bae, J. S., Choo, W. K., Lee, C. H., "The Crystal Structure of Ionic Conductor $La_xCe_{1-X}O_{2-x/2}$", ***Journal of the European Ceramic Society***, Vol. 24, No. 6, (2004), 1291–1294.
8. Ma, W., Ma, Y., Gong, S. K., Xu, H. B., Cao, X. Q., "Thermal Cycling Behavior of Lanthanum-Cerium Oxide Thermal Barrier Coatings Prepared by Air Plasma Spraying", In ***Key Engineering Materials***, Vol. 336, (2007), 1759–1761. Trans Tech Publications Ltd.
9. Zhang, H., Sun, J., Duo, S., Zhou, X., Yuan, J., Dong, S., Yang, X., Zeng, J., Jiang, J., Deng, L., Cao, X., "Thermal and Mechanical Properties of Ta_2O_5 Doped $La_2Ce_2O_7$ Thermal Barrier Coatings Prepared by Atmospheric Plasma Spraying", ***Journal of the European Ceramic Society***, Vol. 39, No. 7, (2019), 2379–2388.
10. Gao, L., Guo, H., Gong, S., Xu, H., "Plasma-Sprayed $La_2Ce_2O_7$ Thermal Barrier Coatings against Calcium–Magnesium–Alumina–Silicate Penetration", ***Journal of the European Ceramic Society***, Vol. 34, No. 10, (2014), 2553–2561.
11. Xu, J., Zhang, Y., Liu, Y., Fang, X., Xu, X., Liu, W., Zheng, R., Wang, X., "Optimizing the Reaction Performance of $La_2Ce_2O_7$-based Catalysts for Oxidative Coupling of Methane (OCM) at Lower Temperature by Lattice Doping with Ca Cations", ***European Journal of Inorganic Chemistry***, Vol. 2019, No. 2, (2019), 183-194.
12. Khademinia, S., Behzad, M., "Lanthanum Cerate ($La_2Ce_2O_7$): Hydrothermal Synthesis, Characterization and Optical Properties", ***International Nano Letters***, Vol. 5, No. 2, (2015), 101–107.
13. Ma, W., Gong, S., Xu, H., Cao, X., "The Thermal Cycling Behavior of Lanthanum–Cerium Oxide Thermal Barrier Coating Prepared by EB–PVD", ***Surface and Coatings Technology***, Vol. 200, No. 16–17, (2006), 5113–5118.
14. Morris, B. C., Flavell, W. R., Mackrodt, W. C., Morris, M. A., "Lattice Parameter Changes in the Mixed-Oxide System $Ce_{1-X}La_xO_{2-x/2}$: A Combined Experimental and Theoretical Study", ***Journal of Materials Chemistry***, Vol. 3, No. 10, (1993), 1007–1013.
15. Andrievskaya, E. R., Kornienko, O. A., Sameljuk, A. V., Sayir, A., "Phase Relation Studies in the CeO_2–La_2O_3 System at 1100–1500 °C", ***Journal of the European Ceramic Society***, Vol. 31, No. 7, (2011), 1277–1283.
16. Zhang, F. X., Tracy, C. L., Lang, M., Ewing, R. C., "Stability of Fluorite-Type $La_2Ce_2O_7$ Under Extreme Conditions", ***Journal of Alloys and Compounds***, Vol. 674, (2016), 168-173.
17. Mote, V. D., Purushotham, Y., Dole, B. N., "Williamson-Hall Analysis in Estimation of Lattice Strain in Nanometer-Sized ZnO Particles", ***Journal of Theoretical and Applied Physics***, Vol. 6, No. 1, (2012), 6.
18. Kurian, M., Kunjachan, C., "Investigation of Size dependency on Lattice Strain of Nanoceria Particles Synthesised by Wet Chemical Methods", ***International Nano Letters***, Vol. 4, No. 4, (2014), 73–80.
19. Liang, S., Broitman, E., Wang, Y., Cao, A., Veser, G., "Highly Stable, Mesoporous Mixed Lanthanum–Cerium Oxides with Tailored Structure and Reducibility", ***Journal of Materials Science***, Vol. 46, No. 9, (2011), 2928–2937.
20. Loche, D., Morgan, L. M., Casu, A., Mountjoy, G., O'Regan, C., Corrias, A., Falqui, A., "Determining the Maximum Lanthanum Incorporation in the Fluorite Structure of La-Doped Ceria Nanocubes for Enhanced Redox Ability", RSC Advances, Vol. 9, No. 12, (2019), 6745-6751.
21. Fichthorn, K. A., "Atomic-Scale Aspects of Oriented Attachment", ***Chemical Engineering Science***, Vol. 121, (2015), 10-15.
22. Wang, F., Richards, V. N., Shields, S. P., Buhro, W. E., "Kinetics and Mechanisms of Aggregative Nanocrystal Growth", ***Chemistry of Materials***, Vol. 26, No. 1, (2014), 5-21.
23. Lv, W., He, W., Wang, X., Niu, Y., Cao, H., Dickerson, J. H., Wang, Z., "Understanding the Oriented-Attachment Growth of Nanocrystals from an Energy Point of View: A Review", ***Nanoscale***, Vol. 6, No. 5, (2014), 2531-2547.
24. Bezkrovnyi, O., Małecka, M. A., Lisiecki, R., Ostroushko, V., Thomas, A. G., Gorantla, S., Kepinski, L., "The effect of Eu doping on the growth, structure and red-ox activity of ceria nanocubes", ***CrystEngComm***, Vol. 20, No. 12, (2018), 1698-1704.
25. Lin, M., Fu, Z. Y., Tan, H. R., Tan, J. P. Y., Ng, S. C., Teo, E., "Hydrothermal Synthesis of CeO2 Nanocrystals: Ostwald Ripening or Oriented Attachment?", ***Crystal Growth & Design***, Vol. 12, No. 6, (2012), 3296-3303.
26. Deshpande, S., Patil, S., Kuchibhatla, S. V., Seal, S., "Size Dependency Variation in Lattice Parameter and Valency States in Nanocrystalline Cerium Oxide", ***Applied Physics Letters***, Vol. 87, No. 13, (2005), 133113.